7-1-2017

Southward Flow on the Western Flank of the Florida Current

Alexander Soloviev
Nova Southeastern University, <<span class="elink">soloviev@nova.edu

Amy Hirons
Nova Southeastern University, <<span class="elink">hirons@nova.edu

Christopher Maingot
Nova Southeastern University

Cayla Whitney Dean
Nova Southeastern University, <<span class="elink">cd821@nova.edu

Richard E. Dodge
Nova Southeastern University, <<span class="elink">dodge@nova.edu

See next page for additional authors

Authors

Alexander E. Yankovsky
University of South Carolina

Jon Wood
Ocean Data Technologies, Inc.

Robert H. Weisberg
University of South Florida

Mark E. Luther
University of South Florida

Julian P. McCreary
University of Hawaii

Deep-Sea Research Part I 125 (2017) 94–105

Contents lists available at ScienceDirect

Deep-Sea Research Part I

journal homepage: www.elsevier.com/locate/dsri

Southward flow on the western flank of the Florida Current

Alexander V. Soloviev[a,*], Amy Hirons[a], Christopher Maingot[a], Cayla W. Dean[a], Richard E. Dodge[a], Alexander E. Yankovsky[b], Jon Wood[c], Robert H. Weisberg[d], Mark E. Luther[d], Julian P. McCreary[e]

[a] Halmos College of Natural Sciences and Oceanography, Nova Southeastern University, Dania Beach, Florida 33004, USA
[b] Marine Science Program and Department of Earth and Ocean Sciences, University of South Carolina, Columbia, South Carolina 29208, USA
[c] Ocean Data Technologies, Inc., Hyannis, Massachusetts 02601, USA
[d] College of Marine Science, University of South Florida, St. Petersburg, Florida 33701, USA
[e] Department of Oceanography, University of Hawaii, Honolulu, Hawaii 96822, USA

ARTICLE INFO

Keywords:
Undercurrent
Surface countercurrent
Western boundary current
Alongshore pressure gradient
Ekman transport
Bottom boundary layer

ABSTRACT

A suite of long-term *in situ* measurements in the Straits of Florida, including the ADCP bottom moorings at an 11-m isobath and 244-m isobath (Miami Terrace) and several ADCP ship transects, have revealed a remarkable feature of the ocean circulation - southward flow on the western, coastal flank of the Florida Current. We have observed three forms of the southward flow - a seasonally varying coastal countercurrent, an undercurrent jet attached to the Florida shelf, and an intermittent undercurrent on the Miami Terrace. According to a 13-year monthly climatology obtained from the near-shore mooring, the coastal countercurrent is a persistent feature from October through January. The southward flow in the form of an undercurrent jet attached to the continental slope was observed during five ship transects from April through September but was not observed during three transects in February, March, and November. This undercurrent jet is well mixed due to strong shear at its top associated with the northward direction of the surface flow (Florida Current) and friction at the bottom. At the same time, no statistically significant seasonal cycle has been observed in the undercurrent flow on the Miami Terrace. Theoretical considerations suggest that several processes could drive the southward current, including interaction between the Florida Current and the shelf, as well as forcing that is independent of the Florida Current. The exact nature of the southward flow on the western flank of the Florida Current is, however, unknown.

1. Introduction

The Florida Current (FC) is a part of the North Atlantic Subtropical Gyre and the western boundary current system, which is represented by the Loop Current in the Gulf of Mexico, continuing as the FC in the Straits of Florida and the Gulf Stream in the North Atlantic (Stommel, 1965). Strong current flow over a rapidly changing three-dimensional topography contributes to the FC's great variety of motions (meandering, eddies, energetic internal tides, etc.) spanning a large range of time and spatial scales. The FC possesses both spatial inhomogeneities related to the topography and mean current structure, and also temporal inhomogeneities related to the local meteorological conditions.

The highly variable influx conditions for five key passages, Grenada, St. Vincent, St. Lucia, Dominica, and Windward Passages, may in part account for the considerable variability of the FC (Wilson and Johns, 1997). Schott et al. (1988) demonstrated that the FC and its variations are subject to both seasonal and interannual variability. Analysis of daily cable transport estimates from a submarine cable from 1982 to 1998 by Meinen et al. (2010) suggests that roughly 70% of the total variance in the FC occurs at periods less than annual.

One potential source of FC variability at periods less than annual includes eddies associated with the western flank of the FC. Lee and Mayer (1977) observed the spin off eddies associated with the western edge of the FC. Shay et al. (2000), Parks et al. (2009), and Archer et al. (2015) conducted observations of surface current manifestations in the nearshore zone with shore-based high-frequency radars, based on phased array principles. These measurements revealed submesoscale eddies, which were initiated by horizontal shear on the western flank of the FC, significantly contributing to short-term variability of nearshore circulation.

Changes in the FC on time periods of 2–20 days are often correlated

* Corresponding author.
E-mail address: soloviev@nova.edu (A.V. Soloviev).

http://dx.doi.org/10.1016/j.dsr.2017.05.002
Received 20 November 2015; Received in revised form 4 May 2017; Accepted 4 May 2017
Available online 18 May 2017

to local winds (Lee and Williams, 1988). Düing et al. (1977) correlated FC variations in the 2–15-day range with atmospheric forcing. The highest correlation was observed between the northward component of the current velocity and *curl* $\vec{\tau}$ (where $\vec{\tau}$ is the wind stress) on time periods of 2.5, 4.5, and 11.8 days. Lee et al. (1985) indicated strong transport variations in the FC in the 2–10-day period correlated with wind stress variations.

Soloviev et al. (2003a, b) reported strong oscillations in the current direction on the Southeast Florida shelf on time scales of approximately 10 h, which were presumably associated with a near-resonant seiching mechanism. Amplitudes of these current velocity oscillations were seasonally modulated with the maximum during late summer.

There have been sporadic observations of an undercurrent below the FC. Düing and Johnson (1971) and Leaman and Molinari (1987) observed strong variations in the current profile in the central and eastern Straits of Florida, resulting in southward flow with speeds up to 0.3 m s^{-1} in the lower half of the water column. Leaman and Molinari (1987) observed an undercurrent on the eastern flank of the FC. To our best knowledge there have been no detailed observations or attempts to simulate southward flow on the western flank of the FC. Such simulations require a higher spatial resolution than available in most regional numerical models.

In our work, we report the observations of the undercurrent and countercurrent in the western part of the Straits of Florida. We have observed three forms of the southward flow - a seasonally varying coastal countercurrent, an undercurrent jet attached to the Florida shelf, and an intermittent undercurrent on the Miami Terrace. The goal of this paper is to report and interpret our observations of the undercurrent and countercurrent on the western, coastal flank of the FC. The paper is organized as follows. Section 2 presents observations in the Straits of Florida. Section 3 provides the analysis of time scales of the ocean circulation variability on the western flank of the FC. Section 4 discusses observations of the coastal countercurrent, the undercurrent jet attached to the continental slope, the vertical structure of the undercurrent jet, and the intermittent undercurrent on the Miami Terrace. Theoretical considerations in Section 5 provide a possible explanation for the southward flow on the western flank of the FC. Section 6 is the discussion, and Section 7 summarizes the results of this work.

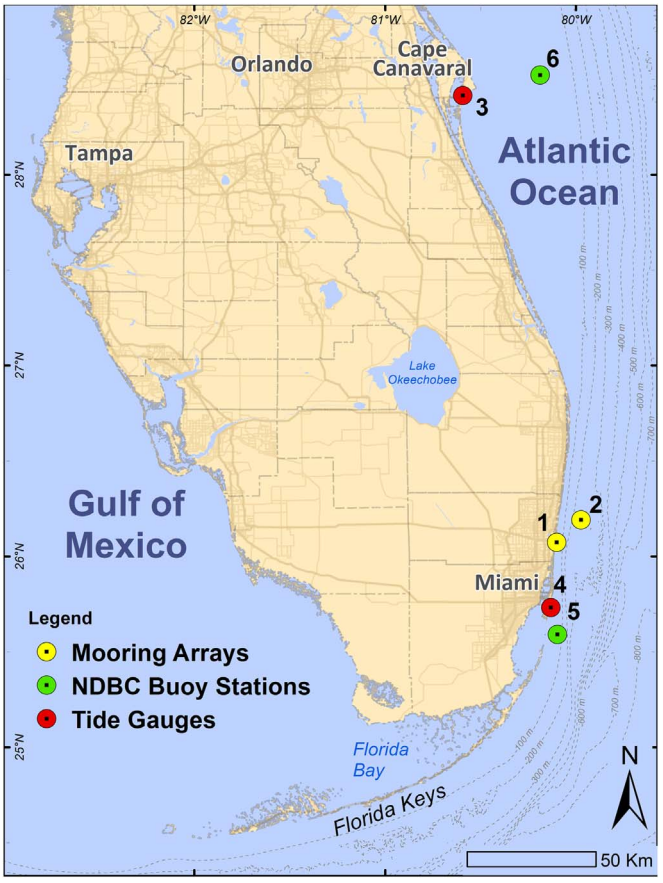

Fig. 1. Location of instruments: Label 1 is the bottom ADCP mooring at an 11-m isobath (26.073°N, 80.101°W); Label 2, the bottom ADCP mooring at a 244-m isobath 8 nautical miles (14.8 km) offshore, which was deployed at 26.191ºN, 79.974°W; Label 3, the Trident Pier tide gauge (28.415°N, 80.593°W); Label 4, the Virginia Key tide gauge (25.732°N, 80.132°W); Label 5, the meteorological station on NDBC Buoy Station FWYF1 - Fowey Rocks, FL (25.591°N, 80.097°W); and Label 6, the meteorological station on NDBC Buoy Station 41009 – Canaveral, 20 NM east of Cape Canaveral, FL (28.522°N, 80.188°W).

2. Observational data

Fig. 1 shows locations of the instruments on the Southeast Florida shelf. The acoustic Doppler current profiler (ADCP) mooring array location is shown in more detail in Fig. 2, superimposed on a synthetic aperture radar (SAR) image. The mooring array consisted of two bottom ADCP moorings deployed at 11-m and 244-m isobaths (Fig. 2). The SAR image indicates the frontal structure on the western flank of the FC. The position of the moorings relative to this frontal structure is also shown in Fig. 2.

The ADCP bottom mooring, deployed on the Dania Beach shelf at the 11-m isobath, has provided almost continuous current velocity data with 0.5 m vertical resolution from June 1999 to May 2013 (Table A1). The ADCP bottom mooring located on the Miami Terrace at the 244-m isobath operated from January 2007 to November 2010 (Table A2). It included a *Flotation Technology* buoy deployed 10 m above the bottom with the following instruments: upward looking Teledyne RD Instruments 75 kHz Long Ranger ADCP measuring vertical profiles of current velocity in the upper water column with 4 m vertical resolution; downward looking Teledyne RD Instruments 300 kHz Workhorse ADCP measuring vertical profiles of current velocity near the seabed with 0.5 m vertical resolution; *Benthos* acoustic modem for communication with the buoy; *Benthos* acoustic release used to facilitate mooring recovery; locator instruments (radio, light, ARGOS satellite). The theoretical standard deviation (accuracy) for the Workhorse and Long Ranger ADCPs due to instrumental uncertainty for hourly samples is given in Table A2. There are three gaps in the time series due to interim mooring servicing, a total of about 58 h of missing data throughout the almost 4-year program.

In addition, seasonal cross-shelf transects were performed in 2007 from the R/V *F.G. Walton Smith* (University of Miami Rosenstiel School of Marine and Atmospheric Science) with the hull-mounted, Teledyne RD Instruments 75 kHz Ocean Surveyor ADCP. The transects shown in Figs. 7–8 ended close to the ADCP mooring located at the 244-m isobath 8 nautical miles offshore.

An additional transect with the station 4 km offshore (Fig. 10) was performed in 2011 from the R/V *Panacea* (Nova Southeastern University Oceanographic Center) using a downward-looking Teledyne RD Instruments 600 kHz Workhorse Monitor ADCP. The ADCP instrument was mounted to an aluminum arm that was raised and lowered into the water from the side of the vessel. Vertical profiles were created by lowering a Valeport Midas 606 CTD instrument through the water column to a depth of approximately 100 m while the vessel was stationary.

During active observational phases, the area was monitored with SAR satellites (see, *e.g.*, Soloviev et al., 2010), which helped to identify the position of the FC front in some cases (Fig. 2). No systematic SAR observations were, however, available during the thirteen years of mooring observations at the 11-m isobath location.

It should be noted that the FC front is not always seen in SAR imagery. In the infrared satellite imagery, the FC and the FC front may also vanish from satellite imagery during the summer months due to

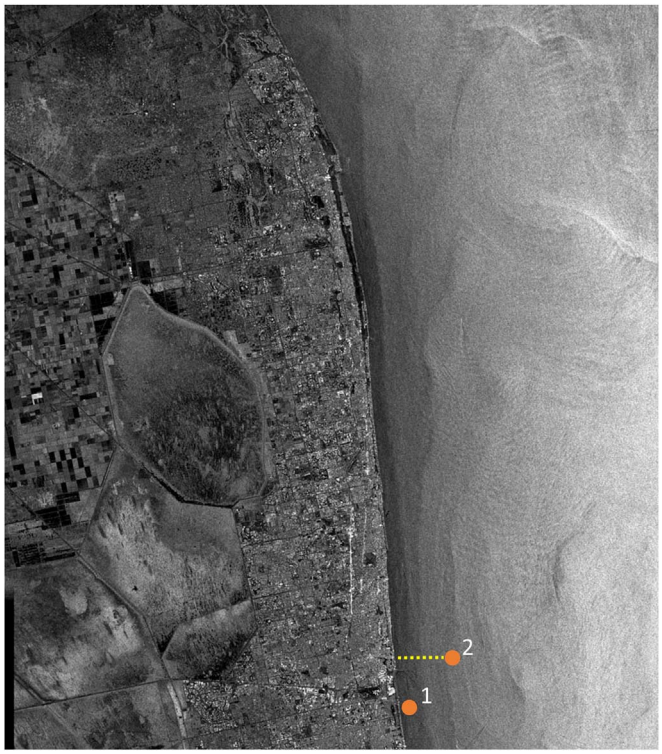

Fig. 2. ADCP mooring locations superimposed on an *ERS-2* satellite SAR image. The SAR image was taken on 19 November 2009; wind speed was 4.9 m s^{-1} and wind direction 348° (meteorological convention). Corner points of the SAR image are 27.088°N, 80.482°W; 26.902°N, 79.486°W; 26.097°N, 80.709°W; 25.912°N, 79.723°W. Label 1 is the bottom ADCP mooring, at an 11-m isobath on the Dania Beach shelf (26.073°N, 80.101°W), and Label 2 is the bottom ADCP mooring 8 nautical miles (14.8 km) offshore at a 244-m isobath (26.191°N, 79.974°W). The dotted line represents the R/V *F.G. Walton Smith* transect repeated approximately every two months (see Figs. 7-8).

decreasing horizontal sea surface temperature gradients under conditions of clear skies and weak winds (Katsaros and Soloviev, 2004; Katsaros et al., 2005).

The strong, highly baroclinic FC is confined to flow over a rapidly changing 3-dimensional topography near Fort Lauderdale, Florida, including the Miami Terrace, which imposes a variety of time and space scales on the FC variability. The bottom topography of the Straits of Florida near Fort Lauderdale is shown in Fig. 3.

Fig. 4 shows the data set of the FC measurements taken from

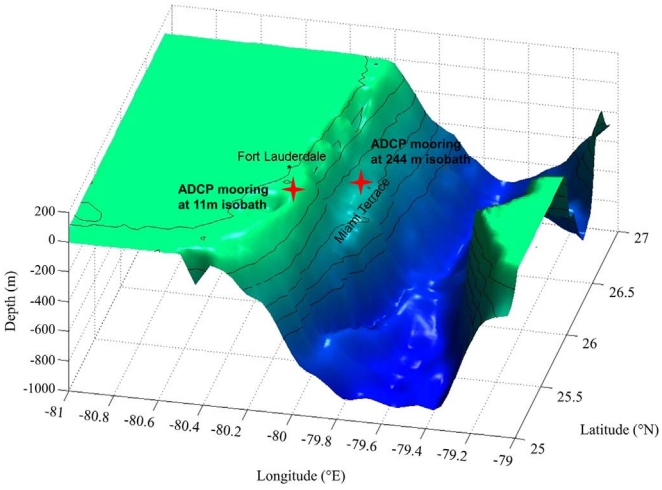

Fig. 3. Bottom topography of the Straits of Florida near Fort Lauderdale, Florida. Locations of the bottom ADCP moorings are shown by four-point stars. The ADCP mooring at the 244-m isobath is located on the Miami Terrace.

January 23, 2007 to September 19, 2010 as a part of the Calypso Liquefied Natural Gas LLC (Calypso LNG LLC) project. The upper subplot shows current velocity speed and the lower subplot, the current direction. Such format provides a more vivid representation of the southward flow than a plot with the vector velocity components, since the northward velocity is typically much larger than the southward velocity. The predominant northward-directed flow throughout the water column was consistent with the presence of the FC. Substantial fluctuations in current magnitude were observed in the upper 150 m. Some high-speed events lasted for just a few days, while others persisted for two weeks or more. This variability is likely explained by lateral meandering or spatial variability of the FC. This mooring at the 244-m isobath was located on the western flank of the FC and the meanders of the FC were obvious in the mooring velocity record. As follows from historical data, meandering is a characteristic feature of the FC, which could be caused by the onshore geostrophic wind component among other factors (see, *e.g.*, Düing et al., 1977).

There are sporadic reversals of the current direction evident from the contour plot of the current direction (Fig. 4). The southward flow is mostly observed in near-bottom layers, though sometimes occupies the entire water column. The near-bottom current reversals are similar to those previously observed by Düing and Johnson (1971) and Leaman and Molinari (1987) in the eastern and central Straits of Florida. The Western Boundary Time Series project from the NOAA Atlantic Oceanographic and Meteorological Laboratory also includes cases of the near-bottom current reversals in the western boundary current at 27°N (http://www.aoml.noaa.gov).

3. Time scales of the circulation variability on the western flank of the Florida Current

A spectral analysis was performed to determine time scales of velocity variability. Fig. 5 shows the variance-preserving spectra of the northward velocity component at four depths. There are significant narrow-banded peaks in the spectra at the diurnal (K1, 23.93 h and O1, 25.82 h) and semi-diurnal (M2, 12.42 h) tidal and inertial (26 h) oscillation periods, but these spikes do not contain a majority of the signal energy. Instead, much of the energy is contained in the subtidal bands (to the left of the curve) at frequencies of about 0.05–0.15 cycles per day, that is, variability at time scales of about 7–20 days. About 90% of the overall signal energy was found in these subtidal frequency bands; the remaining 10% of signal energy was attributed to tides and other higher-frequency variability. This peak separation suggests that lateral meanders of the FC vary at principal time scales of about 1–3 weeks (Fig. 5), which is consistent with observations of Lee (1975).

The results shown in Fig. 5 are consistent with the literature analysis suggesting that the following mechanisms contribute to the FC variability: inertial, tidal and near-tidal oscillations, meandering and eddies (Lee and Mayer, 1977; Mooers, 1975; Mooers and Brooks, 1977; Shay et al., 2000; Parks et al., 2009; Soloviev et al., 2003a; Meinen et al., 2010), as well as wind forcing (Düing et al., 1977; Lee et al., 1985).

4. Coastal countercurrent and undercurrent jet on the western flank of the Florida Current

A remarkable feature of the ocean circulation observed on the western, coastal flank of the FC is the appearance of the southward flow. From the ADCP mooring measurements at an 11-m and 244-m isobath and occasional ship transects, we have identified three forms of the southward flow - a seasonally varying alongshore coastal countercurrent, an undercurrent jet attached to the Florida shelf, and an intermittent undercurrent on the Miami Terrace (Figs. 4, 6–10). Previous sightings of the undercurrents were reported in the eastern and central Straits of Florida (Düing and Johnson, 1971; Leaman and Molinari, 1987).

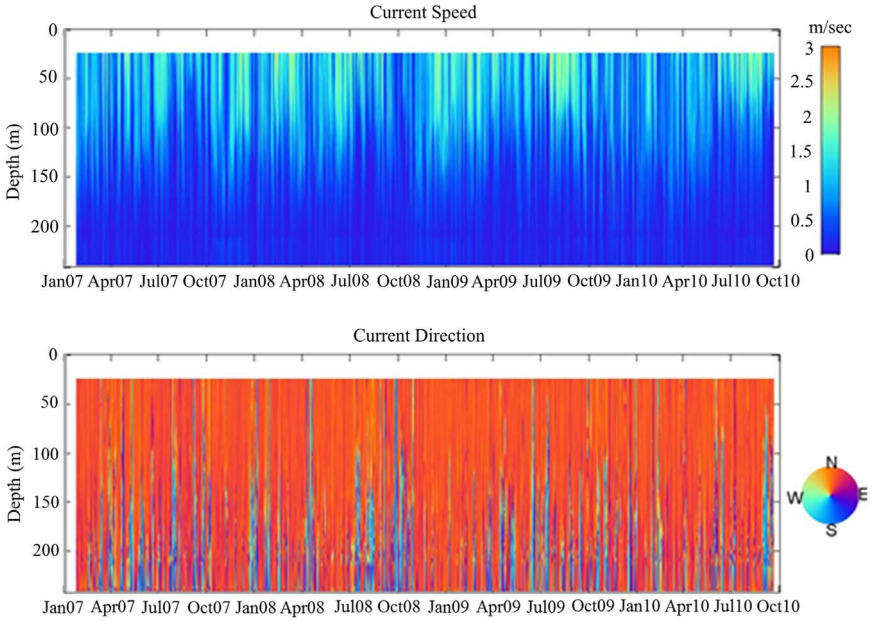

Fig. 4. Current speed and direction 8 nautical miles (14.8 km) offshore at a 244-m isobath (Miami Terrace) from January 23, 2007 to September 19, 2010. Blue shading in the bottom panel indicates the occurrence of southward flow.

4.1. Coastal countercurrent

An approximately 13-year dataset was obtained from an upward looking ADCP instrument deployed at the 11-m isobath on the Dania Beach shelf. The standard deviation of the northward current velocity fluctuations at this location is significantly larger than the averaged current velocity (Table 1). Shedding of submesoscale eddies (Shay et al., 2000), tidal, inertial and near-semidiurnal tidal oscillations contribute to the relatively short-term current variability (Soloviev et al. 2003 a, b). Nevertheless, long-term observations displayed in Fig. 6 as monthly averages reveal a clear seasonal pattern of the coastal currents on the Southeast Florida shelf. The monthly time period has been selected for averaging to suppress the subinertial (7–20 day) and shorter time scales of the current velocity variability that is prominent on the variance-preserving spectra (Fig. 5).

During summer, the mean alongshore current velocity is directed

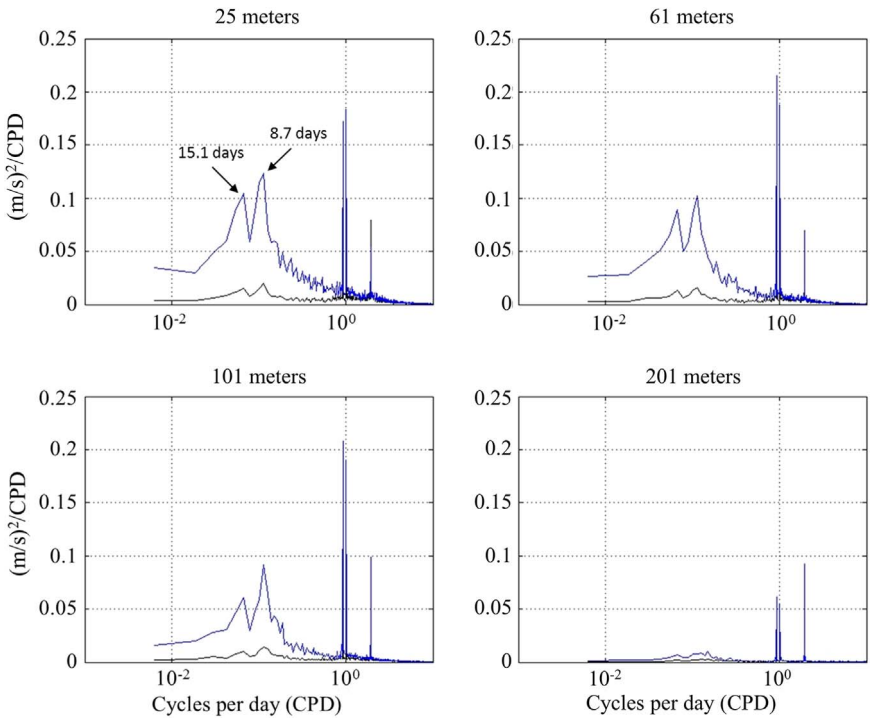

Fig. 5. Variance-preserving spectral plot for 4 discrete depth layers 25 m, 61 m, 101 m and 201 m below the surface (January 2007 through September 2010). Northward flow (blue) was nearly 10x more energetic than eastward flow (black). Spectral peaks close to the 1- and 2-cycles per day frequencies reflect diurnal and semi-diurnal tidal components and inertial oscillations (period of inertial oscillations at this latitude is approximately 26 hours). A majority of the signal energy was found in sub-tidal bands at periods of 7–20 days.

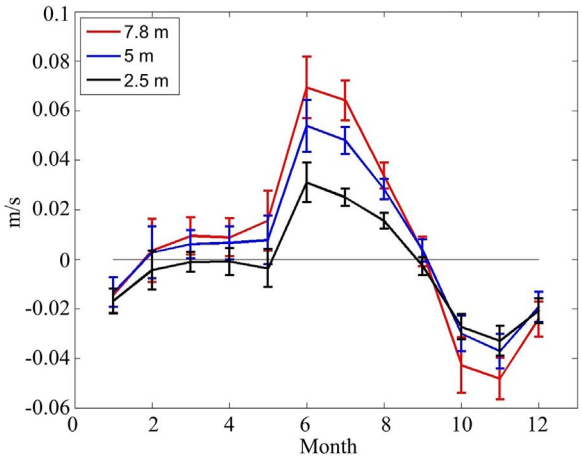

Fig. 6. Seasonality of the northward current velocity component at the 11-m isobath mooring (26.073°N, 80.101°W): Monthly mean current climatology produced by averaging over thirteen years of data with 68% confidence intervals. In the calculation of error bars, we assumed that monthly averages from each year were statistically independent. In the legend 7.8 m, 5 m and 2.5 m refer to height above the bottom.

northwards; whereas during autumn the mean current velocity changes course and is directed southwards. During winter and spring, the mean current velocity is relatively weak and there is much less vertical shear in the water column than during the summer and autumn time (Fig. 6).

4.2. Undercurrent jet on the Southeast Florida shelf

Observations from ship transects shown in Figs. 7–8 reveal the undercurrent jet attached to the Southeast Florida shelf. (We use the convention of 0° to represent northward current direction in all figures.) Fig. 7a reveals a southward jet (green shaded region in the right panel) attached to the continental slope (Fig. 7b) that attained a maximum speed of 0.25 m s^{-1} in April 2007. A similar southward jet over the shelf was observed during cross-shelf transects performed in May, June, September 2007 (Fig. 8), and July 2011 (Fig. 10). The jet appears to vary somewhat in position and strength. Remarkably, in the cross-sections shown in Figs. 7,8, and 10, this jet underneath the FC abutted the continental shelf topography, which can be due to the Coriolis force deflecting the jet toward the continental slope.

In November 2007, however, the southward undercurrent jet was no longer found on the continental slope (Fig. 8). It is possible that it migrated to the surface and contributed to the development of the coastal countercurrent or retreated offshore. There is no indication of either undercurrent or countercurrent on the contour plot taken in February 2007 (Fig. 8). (During the March 2007 cross-section transect, the ship did not approach close enough to the shore to see if a coastal countercurrent was present.) These findings are consistent with the monthly coastal current statistics collected at an 11-m isobath in February and March (Fig. 6).

4.3. Intermittent undercurrent on the Miami Terrace

Reversals of the current direction were periodically observed on the Miami Terrace in deeper layers by the mooring located 8 nautical miles (14.8 km) offshore at the 244-m isobath (Fig. 4). Fig. 9a shows the fraction of time when the near-bottom current on the Miami Terrace at 16 m height above the bottom was flowing southward. This fraction was approximately between 10% and 30% with a maximum in September and a minimum in November.

The seasonal cycle of the southward flow on the Miami Terrace is not so pronounced as in the case of the near shore, 11-m isobath data. This is confirmed by monthly averages of the near-bottom current at the 244-m isobath, 16 m above the bottom (Fig. 9b). The data set at the 244-m isobath, however, is only four years long compared to the 13-year data set collected at the 11-m isobaths (Fig. 6). From the existing data, it is therefore difficult to see any connection between the observations at the 11-m and 244-m isobaths. Spatial separation between these mooring locations can also be a factor.

4.4. Vertical structure of the undercurrent jet

The cross-shelf transect, performed in July 2011 from the R/V *Panacea* also revealed the undercurrent jet attached to the Florida continental slope approximately 4 km offshore (Fig. 10). In order to increase the vertical resolution of velocity measurements, in this experiment a 600 kHz ADCP was used. At this frequency, the maximum depth range was, however, limited to approximately 75 m. A vertical CTD cast was taken in parallel to the ADCP measurement at the undercurrent jet location (indicated by the white vertical dashed line in Fig. 10). The gradient Richardson number shown in Fig. 11 was calculated from the current velocity and density profiles. The velocity profile shows the presence of an undercurrent (change in the current direction to southward flow) below 60 m (Fig. 11, left panel), which is on the order of 0.1 m s^{-1}. According to the density profile (Fig. 11, middle panel), in the upper 20 m there is a surface mixed layer, which is partially stratified, and a relatively well-mixed bottom boundary layer below 60 m depth. Strong shear at the top of the jet and friction of the jet with the ocean bottom contribute to mixing of this undercurrent jet. The jet interaction with the bottom potentially explains the development of the bottom mixed layer, in which the Richardson number drops below its critical value $Ri_{cr} = 0.25$ (Fig. 11, right panel). Mixing intensity in the bottom mixed layer is possibly even higher than in the upper-ocean mixed layer, as indicated by the vertical profile of the Richardson number. There is a pycnocline between 20 and 50 m, which likely suppresses turbulent mixing and thus effectively isolates the undercurrent from the northward-directed surface current (Fig. 11).

5. Theoretical considerations

5.1. Alongshore pressure gradient

Coastal dynamics on monthly or longer time scales affected by vertical eddy viscosity can be described in terms of the arrested topographic wave (ATW) theory (Csanady, 1978). In this theory, the alongshore pressure gradient (APG) force represents an important forcing mechanism for alongshore coastal currents. Numerous observational studies (*e.g.*, Lentz, 1994; Yankovsky, 2003; Batifoulier et al., 2012) revealed that the APG force is often the leading term in the alongshore momentum balance. Below we will estimate an alongshore, depth-averaged momentum balance for the South Florida inner shelf in the water column of O(10 m). From this estimate, we will also infer the possible contribution of APG in generating the observed coastal countercurrent.

For the interpretation of observed currents at the 11-m isobath mooring (Fig. 6), we apply shallow water equations with constant seawater density. For monthly-averaged currents, the local acceleration (inertia) term is assumed to be small compared to the leading order terms. The advective acceleration is also neglected because both the coastline and bathymetry are fairly uniform alongshore in the vicinity of the measurement site (rendering a small alongshore derivative of the alongshore velocity component). These assumptions yield the following momentum balance:

$$-g\frac{\partial \eta}{\partial y} + \frac{\tau_y - C_d v|v|}{\rho H} = 0 \quad (1)$$

where g is the acceleration due to gravity, η is the sea level perturbation, y is the alongshore coordinate, τ_y is the wind stress alongshore

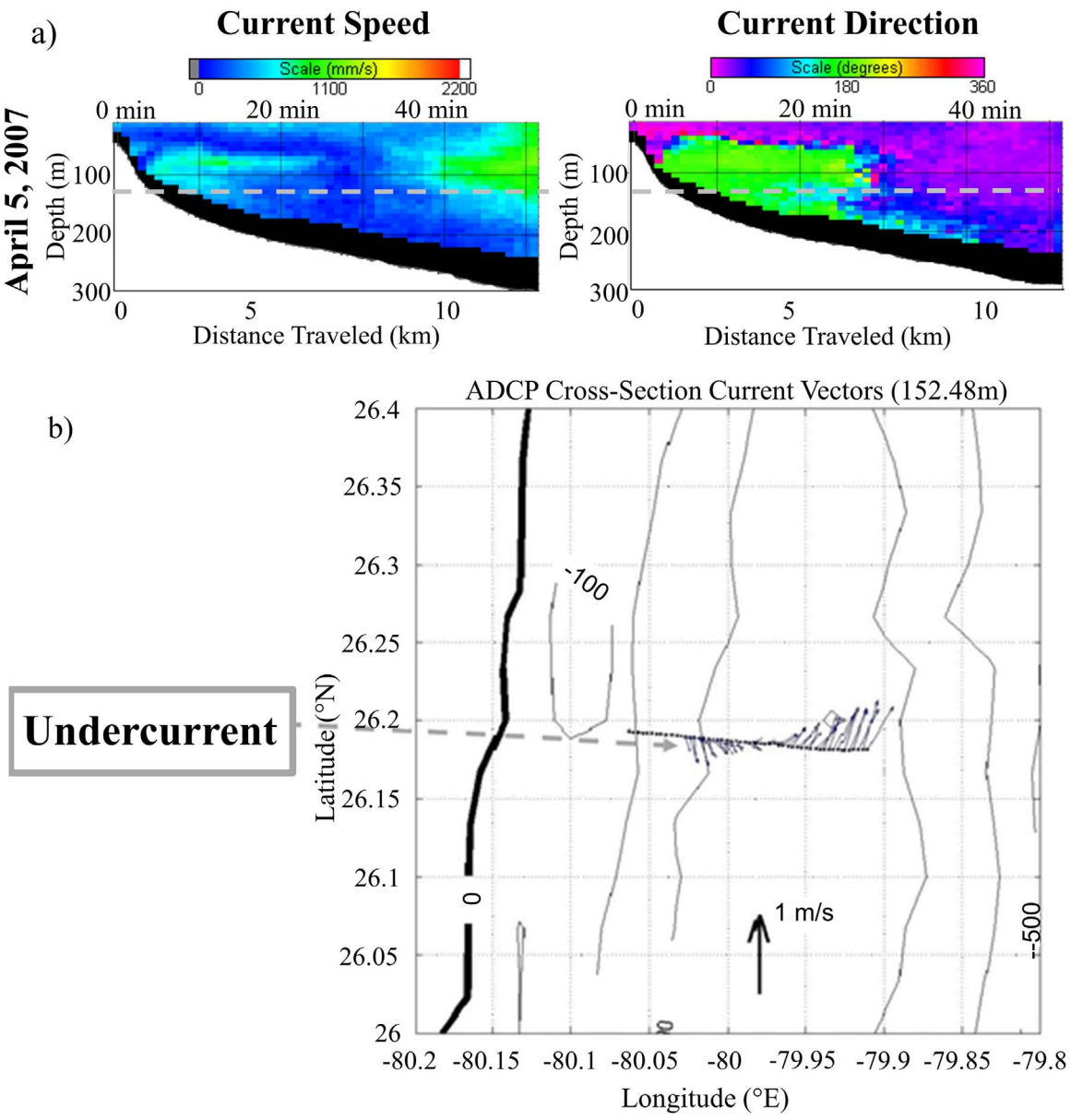

Fig. 7. (a) Cross-shelf transect taken by the R/V *F.G. Walton Smith* on April 5, 2007, revealing the southward undercurrent jet roughly parallel to isobaths. The near-bottom area is blacked-out because of multiple reflections (also in Fig. 8). The green shading in the right panel indicates the region of southward flow. (b) The velocity vector plot on the lower panel corresponds to dashed lines on upper panels. The processing of the ADCP data included decimation by a factor of 10 using the corresponding Matlab function.

component, C_d is the bottom drag coefficient, v is the alongshore velocity component, H is the water depth, and ρ is the water density. Thus, the momentum balance is assumed between the APG force and the difference of surface and bottom shear stresses. Eq. (1) is similar to the alongshore momentum balance considered by Csanady (1978), except the Coriolis force is neglected in our case due to the proximity of the coastline (coastal boundary condition of no normal flow).

The monthly-averaged wind stress for 1999–2013 was derived from the NDBC Buoy 41009 measurements following the Large and Pond (1981) approach (Fig. 12a). For consistency with the monthly averages of sea level perturbations, the wind stress was also calculated from monthly-averaged wind data. An alternative procedure of calculating wind stress from hourly data and then calculating the monthly-averaged wind stress resulted in the "leakage" of high-frequency variability into a monthly-mean, which reduced correlation between the monthly-averaged wind stress and monthly-averaged sea level. We obtained monthly sea level perturbations from sea level measurements at two NOAA tide-gauge stations, Trident Pier (Central Florida, near Cape Canaveral) and Virginia Key (South Florida) (Fig. 1), and averaged them over a 15-year interval (1999–2013). The perturbations are almost identical at both locations during December–April, but differ during June–November (Fig. 12b). The APG force was derived from the sea level difference between the two stations assuming their spatial separation of 400 km. Both APG and wind stress forces generate northward coastal flow in June-August and southward flow in September-November (Fig. 12c), in agreement with the climatology shown in Fig. 6.

Next, we solve (1) for v and compare this estimate with observations. In order to match maximum absolute values of the observed depth-averaged currents ($\sim 5\times10^{-2}\,\mathrm{ms}^{-1}$ – see Fig. 6), we set $C_d = 0.01$. This is a rather high value; however, elevated values of bottom drag coefficient are often observed in the nearshore zone due to the impact of orbital velocities of the surface gravity wave field (Grant and Madsen, 1979). For instance, Garvine (2004) found a record-mean

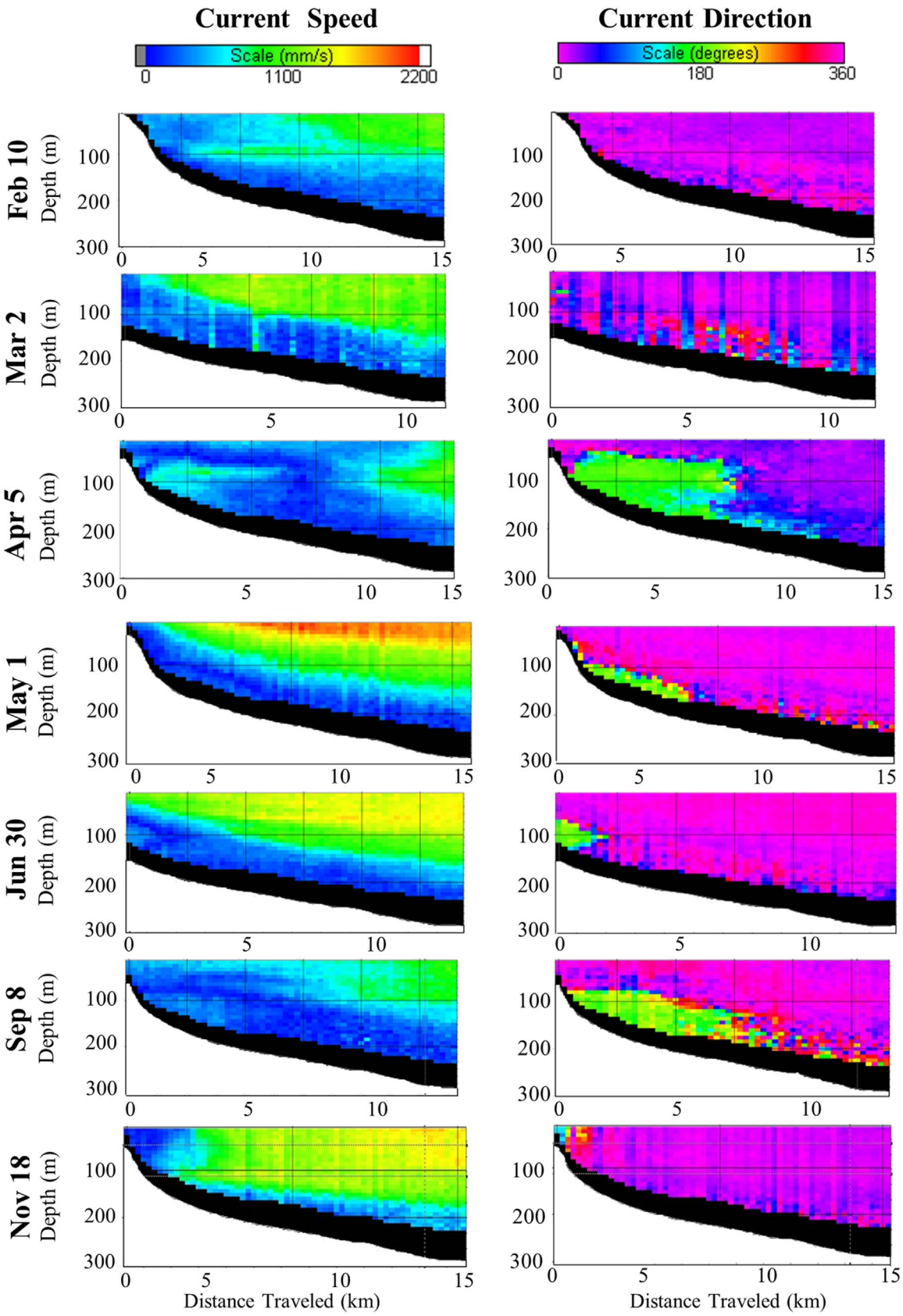

Fig. 8. Cross-shelf transect taken by the R/V *F.G. Walton Smith* on February 10, March 2, April 5, May 1, June 30, September 8, and November 18, 2007, revealing the southward undercurrent jet. The green shading on the right panels indicates the regions of southward flow. The processing of the ADCP data included decimation by a factor of 10 using the corresponding Matlab function.

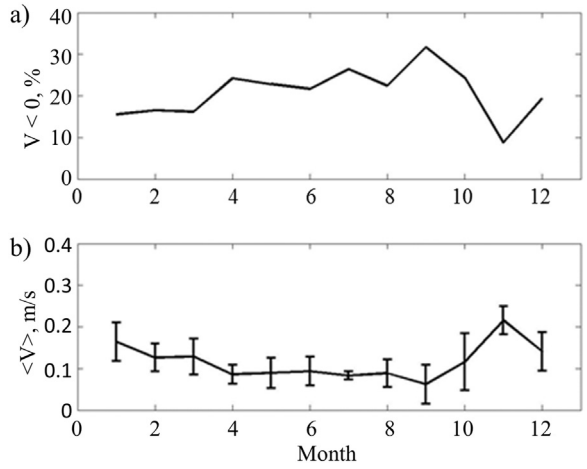

Fig. 9. Seasonality of the northward current velocity component at the 244-m isobath (26.032ºN, 79.994°W). a) Fraction of time when the near-bottom current (determined from the 16 m height above the bottom) was flowing southward (VMonthly mean current climatology of the near-bottom current produced by averaging over four years of data with 70% confidence intervals. In the calculation of error bars, we assumed that monthly averages from each year were statistically independent and also applied the Student's t-distribution (Emery and Thomson, 2004).

value for C_d to be 0.026 on the New Jersey shelf, an even higher value than what is applied here in our estimates. While the estimated v does not match observed depth-averaged velocity perfectly, it does capture major patterns of the observed temporal evolution: the northward flow in the summer and the southward flow in the autumn (Fig. 12d). Of the two driving forces included in the momentum balance, APG force is believed to have higher absolute values than the wind stress (Fig. 12c). Remember that the APG calculated from the difference between Trident Pier and Virginia Key may or may not exactly represent that at the Dania Beach mooring site, depending on the forcing conditions, presence of mesoscale dynamics on the shelf, *etc.* Therefore, the error in the APG estimation for the local momentum balance might not be related to the statistical properties of sea level measurements at the two locations. Note that in general the error bars are seldom put on the momentum balance term estimations (*e.g.*, Lentz et al., 1999).

This observed APG operates in a different manner when compared to the "typical" APG induced on continental shelves by the regional wind forcing. When the atmospheric system affects the coastal ocean under a typical scenario, an APG is set up after the passage of coastal trapped waves originating from the northward (in the sense of Kelvin-wave propagation) edge of the atmospheric system (*e.g.*, Carton, 1984). Such an APG force opposes the direction of the alongshore wind stress. Furthermore, the amplitude of the wind-forced perturbation increases southward in the case of the US East Coast (*e.g.*, Yankovsky and Garvine, 1998). Under this conventional scenario, the APG force has a tendency to generate a countercurrent relative to the direction of the

Table 1
Annually averaged northward velocity component and standard deviation from the 11-m isobath bottom mooring.

Height above bottom (m)	Annual averaged northward velocity component (m s^{-1})	Standard deviation (m s^{-1})
7.8	0.004	0.18
5.0	0.002	0.16
2.5	−0.005	0.14

regional alongshore wind stress (Lentz, 1994; Yankovsky, 2003). The opposite relationship seems to hold in the example in Fig. 12: A southward APG force develops in September–November when the alongshore wind stress points in the same direction so that the southward coastal current is driven simultaneously by the APG and the wind stress. Prevailing downwelling conditions during this time interval are further evident in the high sea level anomaly at the coast.

One possibility for the observed APG generation is through remote forcing (DiNezio et al., 2009, Domingues et al., 2016). Czeschel et al. (2012) studied the annual cycle of the FC transport and found that remotely generated long barotropic waves propagating southward along the North American coast contribute to the FC transport anomalies (up to ~1 Sv). However, a good agreement between the regional wind stress and APG (Fig. 12) suggests that the regional wind forcing can also contribute to the observed APG, but through a different mechanism than the coastally trapped wave propagation described above. This mechanism is discussed in the next section.

5.2. Wind stress effects

The coastal countercurrent (see Fig. 6) has a maximum during the autumn and is consistent with the APG and wind stress forces (Fig. 12c). Interestingly, the APG-induced component of the countercurrent has a larger magnitude but the same sign as the wind stress-induced component (Fig. 12d). We propose the following hypothesis for this abnormal regime. The onshore Ekman transport can be modified by the area of strong cyclonic vorticity associated with the FC western flank. Kunze (1985) suggested that the local inertial frequency can be modified in the presence of strong geostrophic shear as $f' = f + \xi/2$, where $\xi = V_x - U_y$ is the relative vorticity associated with the mean flow (where subscripts denote the differentiation with respect to x and y, respectively). Indeed, Shearman (2005) observed this effect in near-inertial oscillations on the New England shelf in the presence of persistent anticyclonic relative vorticity. In our case, the Ekman transport on the shelf is modified by the FC to be,

$$U_E = \frac{\tau_y}{\rho(f + V_x)}, \tag{2}$$

where τ_y is the meridional wind stress component. This argument implies that positive (cyclonic) vorticity on the FC western flank can increase the effective inertial frequency and consequently reduce the

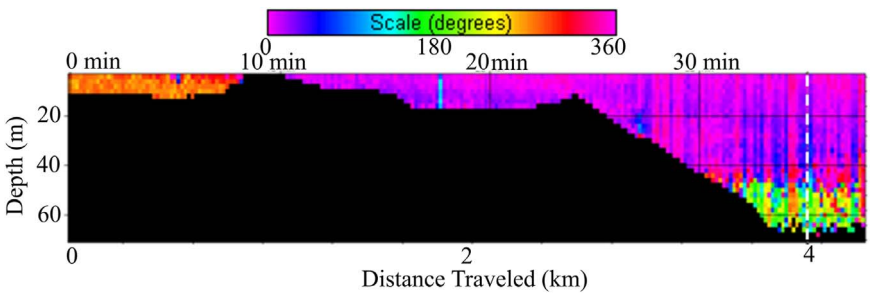

Fig. 10. Cross-shelf transect near Port Everglades, Florida on July 16, 2011, showing velocity direction with purple shading indicating northward flow and green shading indicating southward flow. The orange shading (near the shore) indicates westward tidal flow. The blue vertical line at approximately 1.8 km is due to crossing the wake of a large ship.

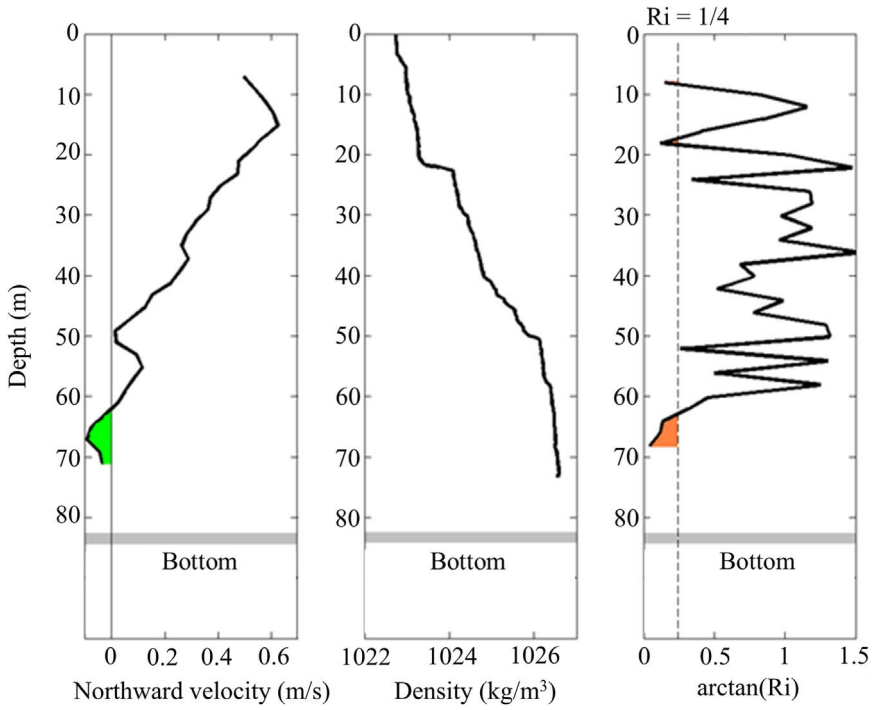

Fig. 11. The vertical structure of the southward flow below the FC, showing velocity (left), density (middle), and Richardson number (right). For convenience of presentation of both positive and negative values as well as very large positive values, the Richardson number dependence is shown in the arctangent coordinate. The green color in the left subplot and the orange color in the right subplot indicate the presence of an undercurrent jet. The dashed vertical line on the right subplot corresponds to $Ri_{cr} = 0.25$.

onshore Ekman transport associated with southward winds. Mooring measurements across the FC (*e.g.*, Fig. 5 in Leaman et al., 1987; and Fig. 3 in Seim et al., 1999) demonstrate that the near-surface cyclonic vorticity on the FC western flank at 100–200 m isobath exceeds

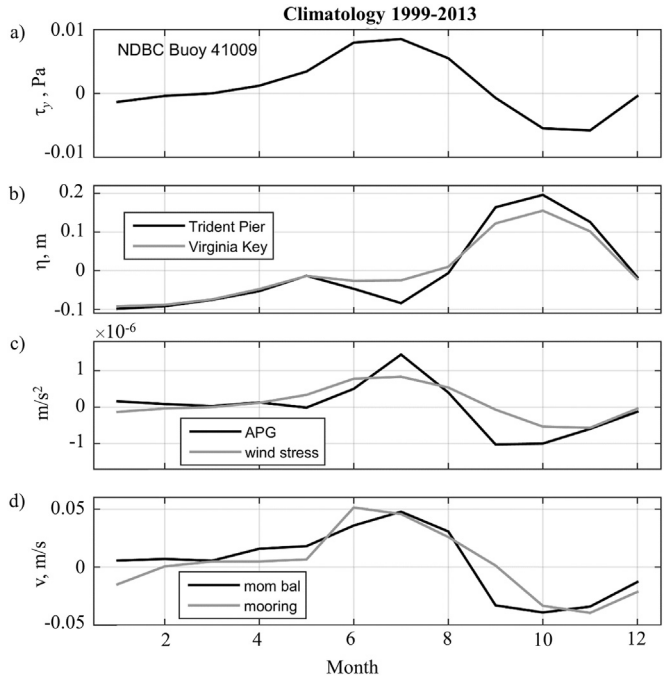

Fig. 12. (a) (a) Monthly-averaged meridional component of wind stress from NDBC Buoy Station 41009 – Canaveral, 20 NM east of Cape Canaveral, FL (28.522°N and 80.188°W), (b) sea level perturbation from the record mean at Trident Pier and Virginia Key tide gauge stations, (c) estimates for the APG and wind stress forces, (d) the alongshore velocity estimate based on the momentum balance (1) (black line) and the depth-averaged climatology (grey line).

$5\times10^{-5}\,s^{-1}$, which is comparable to the Coriolis parameter at 26°N of $6.39\times10^{-5}\,s^{-1}$. The additive effect of the FC relative vorticity to the local inertial frequency can reduce the Ekman transport almost in half. Similar reduction of the Ekman transport by positive vorticity in the Monterey Bay was reported by Woodson (2013). This effect will be much stronger in the southern part of the Florida shelf (due to the proximity of the FC) and it will be negligible further to the north where there is a wide separation between the inner shelf and the FC. The net result will be a larger positive sea level anomaly in the north and, hence, a southward pressure-gradient force. Note, as the "effective" inertial frequency increases, the Ekman layer thickness decreases and nonlinear effects can alter the Ekman layer dynamics (Brink 1997) so we do not attempt to directly estimate a sea level anomaly associated with the FC shear.

5.3. Interaction of FC with shelf

Assuming a near-steady regime, the shelf response to the offshore forcing can be described in terms of the ATW theory (Csanady, 1978). This theory utilizes an analogy between the steady-state frictional shelf circulation and the heat conductivity equation. In particular, in the ATW solution, the direction of Kelvin-wave propagation is analogous to time. That is, the response spreads across the shelf with respect to the downstream distance. It implies that the low pressure anomaly set by the FC at the shelfbreak will penetrate further inshore in a southward direction. The net result will be the establishment of an alongshelf pressure-gradient field. Similar mechanisms were invoked in order to describe a circulation induced on the West Florida shelf by the Loop Current (Hetland et al., 1999) and by the baroclinic "rim" jet which detaches from the Loop Current and flows northward over the continental slope (Hetland et al., 2001). The lateral spreading of the shelf current caused by bottom friction can be limited under stratified conditions by the buoyancy arrest of the bottom boundary layer (*e.g.*, Chapman and Lentz, 1997; Brink, 2012, among many others). Hence, we expect to see a seasonal cycle in this mechanism, following the

development of stratification on the Florida shelf.

The ATW effect can be further amplified by the East Florida shelf geometry. It widens substantially to the north, which further decouples the North Florida inner shelf from the low pressure anomaly at the shelfbreak set by the FC. In contrast, the southern inner shelf becomes more exposed to the low-pressure anomaly due to its proximity to the FC. This geometry will further enhance the decrease of pressure along the coastline in the southward direction.

The problem of interactions of the FC with the shelf has many aspects. However, some details are still unknown due to the lack of proper observations on the southeastern Florida shelf.

6. Discussion

According to our long-term observations, the southward flow on the western flank of the FC appears sometimes as a surface countercurrent and at other times as an undercurrent. The countercurrent and undercurrent could be different representations of the same phenomenon under different background conditions (*e.g.*, seasonally modulated stratification). However, they could also be distinct phenomena.

The exact nature of the southward flow on the western flank of the FC is unknown. At this point we do not know whether the current system over the shelf off Fort Lauderdale is local, or rather is characteristic of circulations along the entire Straits of Florida.

Several processes could drive the southward current. They include processes that involve interaction between the FC and the shelf, as well as forcing that is independent of the FC. As suggested by the tide-gauge stations mentioned in Section 5.1, the southward flow is dynamically linked to the large-scale APG field along the shelf. The alongshore pressure gradient can be induced on the East Florida shelf by the FC. Specifically, the FC establishes a low-pressure anomaly along its western flank approximately at the shelfbreak, thereby providing an offshore forcing for southward geostrophic flow on the shelf, which in turn generates a southward pressure-gradient force.

The southward flow can also be generated by the alongshore wind stress over the shelf. This may be applicable to the coastal countercurrent, but quite unlikely for the undercurrent. The coastal countercurrent could also be driven by eddies developing on the western flank of the FC due to strong shear (Shay et al., 2000; Archer et al., 2015).

According to the ship surveys (Figs. 7–8), the undercurrent jet observed during summertime varies in shape and position with time, which can be ascribed to tidal and inertial oscillations. There have been reports that inertial oscillations and tides in this area can be strongly baroclinic, especially during the summer season (see Mooers, 1975; Soloviev et al. 2003a, b, and others).

Stratification and turbulent mixing impact the vertical structure of the southward flow. The existence of an undercurrent requires a stably stratified layer above it (Lu et al., 1998). The stratified layer isolating the undercurrent jet from the FC may disappear during winter time because of increased convective mixing due to surface cooling.

We hypothesize that vertical stratification plays a key role in the southward flow dynamics. During summer months, an undercurrent jet develops beneath the strong pycnocline. Strong stable stratification in the pycnocline results in suppression of turbulence and turbulent friction, which effectively “isolates” the undercurrent jet from the main, northward stream (the FC). Cooling of the sea surface in the coastal waters of the Straits of Florida during winter months (Katsaros and Soloviev, 2004) indicates the weakening of stratification; as a result, turbulent friction in the water column increases, and the undercurrent jet can no longer exist below the main northward flow. The undercurrent jet, nevertheless, can now migrate shoreward by the action of the Coriolis force since the stratification is weak and there is no longer any substantial density (buoyancy) difference in the vertical direction. This hypothesis may explain the seasonal cycle observed at the 11-m isobath and in occasional ship transect data, but not in observations at the 244-m isobath. The later have not revealed any statistically significant seasonal signal.

The volume transport by the southward flow is not large compared to the FC transport. However, a better understanding of the processes that maintain and account for the variability of the southward flow is important for a number of practical applications. The southward flow may affect pollution propagation, including monitoring and forecasting of potential oil spills that can propagate from the Gulf of Mexico through the Loop Current (Goni et al., 2015). It may help to explain propagation of genetic information in the marine ecosystem along the United States Atlantic coast and Caribbean (Johnston and Purkis, 2011). Geological structures in the form of sand ripples indicating currents opposite to the FC direction can be linked to the southward flow (Düing and Johnson, 1971; Gardner et al., 1989). The southward flow must also be a part of the life cycle of deep corals (Reed et al., 2013 and others).

Despite the long history of oceanographic observations in the Straits of Florida, the underlying dynamics of the southward flow on the western flank of FC still remain unclear. Additional studies including long-term observations are required.

7. Conclusions

A prominent feature of the reported long-term observations is the southward flow on the western flank of the FC. The southward flow has been observed based on three distinct datasets, a 13-year ADCP dataset from an 11-m isobath mooring, a 4-year ADCP dataset from a 244-m isobath mooring (Miami Terrace). In addition, the southward flow was found during seven cross-shelf transects by the R/V *F.G. Walton Smith* from February to November 2007, and one by the R/V *Panacea* in July 2010. We have observed three forms of the southward flow - a seasonally varying coastal countercurrent, an undercurrent jet attached to the Florida shelf, and an intermittent undercurrent on the Miami Terrace (Figs. 4, 6–10). According to a 13-year monthly climatology obtained from a near-shore mooring (Fig. 6), a relatively-weak coastal countercurrent is a persistent feature of the ocean circulation on the Southeast Florida shelf from October through January. The southward flow in the form of a well-mixed undercurrent jet following the continental slope topography was observed during the five ship transects from April through September but not during the three transects from November through March. At the same time, the undercurrent flow on the Miami Terrace did not show a statistically significant seasonal cycle.

The development of a coastal countercurrent can be explained by a simple alongshore momentum balance with the APG as the primary driving force. Remarkably, the APG in this case is additive to the wind stress. Further research is needed to understand how this APG is formed, and what role the FC might play in this process.

The western flank of the FC showed flow reversals and significant variability on shorter time scales than one month, which were associated with eddies, tides, inertial oscillations, *etc.* High frequency radar technology (see *e.g.*, Archer et al., 2015) can be useful in future studies of the possible connection of these processes with the dynamics of these flow reversals. In order to verify the seasonal shift in the jet location, multiyear observations should be continued.

Acknowledgements

The ocean observing system on the Southeast Florida shelf was established in 1999 as a cooperative agreement between the NSU Oceanographic Center and USF College of Marine Science, funded by ONR. Excellent technical support was provided by Rick Cole and Jeff Donovan (USF), Terry Thompson, Laslo Nemeth, Brian Ettinger and Lance Robinson (NSU). We thank Patrick Bradley (Teledyne RDI) for providing the Long Ranger ADCP on very short notice. Doug Briggs and Bob Franks (FAU), and SFTF personnel were very helpful with the initial mooring operations and the crew of the towboat *Becker* provided

excellent mooring operations. We also thank Michael Crane (NOAA), Kevin Kohler and Courtney Campbell (NSU), Rebekah Walker (NSU and NOAA), Jenny Fenton (NSU and USF), Naoko Kurata (NSU and Smithsonian Institute), and Luba Solonenko (NSU) for help in preparation of the mooring database (http://nsuworks.nova.edu/occ_facreports/52). The map in Fig. 1 was prepared by Brian Walker (NSU).

We thank William Venezia (SFOMF), Manhar Dhanak (FAU), Nick Shay (UM), Chris Mooers (UM), Silvia Matt (NSU), George Vulgaris (USC) and Lew Gramer (CIMAS) for discussion of the project results and logistical support.

The long-term ADCP mooring deployment was funded by SUEZ Energy North America, Inc. as a part of CALYPSO LNG LLC project. Establishment of the NSU OC Coastal Ocean Mooring System was supported by subcontract to FAU # NR993/97–305 (ONR # N00014-98-1–0861), ONR Award N00014-02-1–0950, and Carnival Cruise Lines. Funding support has also been provided by the SECOORA/South Carolina Sea Grant Consortium, NOAA Award NA08N OS4730409, ONR Award N00014-10-1–0938, CIMAS Award S15-01/AC55653 (NOAA NA10OAR4320143), and the University of Miami/Gulf of Mexico Research Initiative Award S120021: "Consortium for Advanced Research on Transport of Hydrocarbon in the Environment (CARTHE)."

Appendix

See Tables A1 and A2 here.

Table A1
Time line of the ADCP data from the 11 m bottom mooring. The date format is yy/mm/dd.

Date/time of first data (ensemble number)	Date/time of last data (ensemble number)	Ensemble interval (s)	Frequency (Hz)	Sampling standard deviation due to instrument uncertainty (cm s^{-1})
99/06/25 21:00:00 (37)	99/08/10 15:00:00 (4429)	900	300	1.47
99/08/11 12:14:57 (19)	99/10/19 12:14:57 (1675)	3600	300	1.47
99/10/23 17:00:00 (6)	00/04/17 19:00:00 (4256)	3600	300	1.47
00/04/19 19:00:00 (8)	00/11/10 16:00:00 (4925)	3600	300	1.47
01/05/16 15:00:00 (42)	02/02/05 14:00:00 (6401)	3600	300	1.47
02/02/06 21:00:00 (4)	02/10/22 14:00:00 (6189)	3600	300	1.47
02/10/22 18:00:00 (5)	03/06/19 13:00:00 (5760)	3600	600	0.72
03/06/19 16:00:00 (25)	03/12/11 14:00:00 (4223)	3600	600	0.72
03/12/11 17:00:00 (18)	04/06/06 13:00:00 (4286)	3600	600	0.72
04/06/06 15:03:39 (4)	04/06/08 15:03:39 (52)	3600	600	3.43
04/06/08 18:03:39 (55)	04/06/23 13:03:39 (410)	3600	600	3.43
04/06/23 16:08:19 (65)	05/07/22 15:48:19 (28432)	1200	600	1.11
05/07/22 16:35:10 (25)	05/09/17 13:35:10 (16405)	300	600	1.38
05/09/17 17:23:04 (10)	05/11/19 15:08:04 (18127)	300	600	1.38
05/11/19 21:58:56 (26)	06/05/15 12:43:56 (50891)	300	600	1.38
06/06/21 23:05:17 (19)	06/11/19 13:15:17 (43389)	300	600	1.38
06/11/19 19:07:58 (20)	07/04/09 20:22:58 (40643)	300	600	1.38
07/04/09 21:58:22 (46)	07/07/31 22:08:22 (32592)	300	600	1.93
07/07/31 23:43:21 (23)	07/09/12 12:33:21 (12273)	300	600	1.99
07/09/12 17:26:20 (22)	08/03/28 14:26:20 (57010)	300	600	1.93
08/03/28 21:29:31 (24)	08/07/14 15:09:31 (31052)	300	600	1.93
08/09/17 18:16:33 (20)	09/01/19 14:51:33 (35691)	300	600	1.93
09/01/19 21:36:23 (23)	09/06/15 12:46:23 (42253)	300	600	1.93
09/06/15 22:07:43 (21)	09/08/17 16:37:43 (18099)	300	600	1.93
09/12/09 18:57:42 (24)	10/04/06 09:07:42 (33890)	300	600	1.93
10/07/30 16:21:36 (22)	10/09/27 11:06:36 (16951)	300	600	1.93
11/06/14 13:30:00 (13)	11/08/1015:04:59 (16448)	300	600	1.93
11/08/10 18:15:29 (9)	12/03/18 01:20:29 (63454)	300	600	1.93
12/11/07 15:25:00 (54)	13/05/03 14:29:59 (51019)	300	600	1.93

Table A2
Time line of the ADCP data from the 244 m bottom mooring. The date format is yy/mm/dd. Note the upward oriented ADCP is the 75 kHz Longranger and the downward oriented ADCP is the 300 kHz WorkHorse.

Date/time of first data (ensemble number)	Date/time of last data (ensemble number)	Ensemble interval (s)	Orientation	Sampling standard deviation due to instrument uncertainty (cm s^{-1})
07/01/23 23:00:00 (9)	07/06/15 12:00:00 (3430)	3600	Upward	1.61
07/01/23 22:40:00 (10)	07/06/15 12:40:00 (10276)	1200	Downward	3.60
07/06/15 20:00:00 (5)	07/11/28 13:00:00 (3982)	3600	Upward	1.61
07/06/15 18:00:00 (6)	07/11/28 14:40:00 (11948)	1200	Downward	3.60
07/11/29 16:00:00 (11)	08/11/20 12:00:00 (8575)	3600	Upward	1.61
07/11/29 16:00:00 (11)	08/11/20 10:00:00 (8573)	3600	Downward	2.08
08/11/21 16:00:00 (17)	10/09/19 22:00:00 (16031)	3600	Upward	1.61
08/11/21 16:00:00 (17)	10/11/16 09:00:00 (17410)	3600	Downward	2.08

References

Archer, M.R., Shay, L.K., Jaimes, B., Martinez-Pedraja, J., 2015. Observing frontal instabilities of the Florida Current using high frequency radar. In: Liu, Y., Kerkering, H., Weisberg, R.H. (Eds.), Coastal Ocean Observing Systems: Advances and Syntheses. Elvsevier.

Batifoulier, F., Lazure, P., Bonneton, P., 2012. Poleward coastal jets induced by westerlies in the Bay of Biscay. J. Geophys. Res. 117, C03023. http://dx.doi.org/10.1029/2011JC007658.

Brink, K.H., 1997. Time-dependent motions and the nonlinear bottom Ekman layer. J. Marine Res. 55, 613–631.

Brink, K.H., 2012. Buoyancy arrest and shelf-ocean exchange. J. Phys. Oceanogr. 42, 644–658.

Carton, J.A., 1984. Coastal circulation caused by an isolated storm. J. Phys. Oceanogr. 14, 114–124.

Chapman, D.C., Lentz, S.J., 1997. Adjustment of stratified flow over a sloping bottom. J. Phys. Oceanogr. 27, 340–356.

Csanady, G.T., 1978. The arrested topographic wave. J. Phys. Oceanogr. 8, 47–62.

Czeschel, L., Eden, C., Greatbatch, R.J., 2012. On the driving mechanism of the annual cycle of the Florida Current transport. J. Phys. Oceanogr. 42, 824–839.

DiNezio, P.N., Gramer, L.J., Johns, W.E., Meinen, C.S., Baringer, M.O., 2009. Observed interannual variability of the Florida Current: wind forcing and the North Atlantic Oscillation. J. Phys. Oceanogr. 39, 721–736.

Domingues, R., Baringer, M., G, Goni, 2016. Remote sources for year-to-year changes in the seasonality of the Florida Current transport. J. Geophys. Res.: Oceans 121, 7547–7559.

Düing, W., Johnson, D., 1971. Southward flow under the Florida. Curr. Sci. 173, 428–430.

Düing, W., Mooers, C.N.K., Lee, T.N., 1977. Low frequency variability in the Florida Current and relations to atmospheric forcing from 1972 to 1974. J. Mar. Res. 35, 129–161.

Emery, W.J., Thomson, R.E., 2004. Data Analysis Methods in Physical Oceanography. Elsevier, Amsterdam (et al., 638 pp).

Gardner, W.D., Richardson, M.J., Cacchione, D.A., 1989. Sedimentological effects of strong southward flow in the Straits of Florida. Mar. Geol. 86, 155–180.

Garvine, R.W., 2004. The vertical structure and subtidal dynamics of the inner shelf off New Jersey. J. Mar. Res. 62, 337–371.

Goni, J.G., Trinanes, J.A., MacFadyen, A., Streett, D., Olascoaga, M.J., Imhoff, M.L., Muller-Karger, F., Roffer, M.A., 2015. Variability of the Deepwater Horizon surface oil spill extent and its relationship to varying ocean currents and extreme weather conditions, in Mathematical Modelling and Numerical Simulation of Oil Pollution Problems, Editor Matthias Ehrhardt, Ch. 1, 1-22.

Grant, W.D., Madsen, O.S., 1979. Combined wave and current interaction with a rough bottom. J. Geophys. Res. 84, 1797–1808.

Hetland, R.D., Hsueh, Y., Leben, R.R., Niiler, P.P., 1999. A Loop Current-induced jet along the edge of the West Florida shelf. Geophys. Res. Lett. 26, 2239–2242.

Hetland, R., Hsueh, Y., Yuan, D., 2001. On the decay of a baroclinic jet flowing along a continental slope. J. Geophys. Res. 106, 19,797–19,807.

Johnston, M.W., Purkis, S.J., 2011. Spatial analysis of the invasion of lionfish in the western Atlantic and Caribbean. Mar. Poll. Bull. 62, 1218–1226.

Katsaros, K.B., Soloviev, A.V., 2004. Vanishing horizontal sea surface temperature gradients at low wind speeds. Bound.-Layer. Meteorol. 112, 381–396.

Katsaros, K.B., Soloviev, A.V., Weisberg, R.H., Luther, M.E., 2005. Reduced horizontal sea surface temperature gradients under conditions of clear sky and weak winds. Bound.-Layer. Meteorol. 116, 175–185.

Kunze, E., 1985. Near-inertial wave propagation in geostrophic shear. J. Phys. Oceanogr. 15, 544–565.

Large, W.G., Pond, S., 1981. Open ocean momentum flux measurements in moderate to strong winds. J. Phys. Oceanogr. 11, 324–336.

Leaman, K.D., Molinari, R.L., Vertes, P.S., 1987. Structure and variability of the Florida Current at 27°N: april 1982 July 1984. J. Phys. Oceanogr. 17, 565–583.

Leaman, K.D., Molinari, R.L., 1987. Topographic modification of the Florida Current by Little Bahama and Great Bahama Banks. J. Phys. Oceanogr. 17, 1724–1736.

Lee, T.N., 1975. Florida current spin-off eddies. Deep-Sea Res 22, 753–765.

Lee, T.N., Mayer, D.A., 1977. Low-frequency current variability and spin-off eddies on the shelf off southeast Florida. J. Mar. Res. 35, 193–220.

Lee, T.N., Scott, F.A., Zantopp, R.J., 1985. Florida Current: low-frequency variability as observed with moored current meters during April 1982 to June 1983. Science 227, 298–302.

Lee, T.N., Williams, E., 1988. Wind-forced transport fluctuations of the Florida Current. J. Phys. Oceanogr. 18, 937–946.

Lentz, S.J., 1994. Current dynamics over the Northern California inner shelf. J. Phys. Oceanogr. 24, 2461–2478.

Lentz, S., Guza, R.T., Elgar, S., Feddersen, F., Herbers, T.H.C., 1999. Momentum balances on the North Carolina inner shelf. J. Geophys. Res. - Oceans 104, 18205–18226.

Lu, P., McCreary, J.P., Klinger, B.A., 1998. Meridional circulation cells and the source waters of the Pacific Equatorial Undercurrent. J. Phys. Oceanogr. 28, 62–84.

Meinen, C.S., Baringer, M.O., Garcia, R.F., 2010. Florida Current transport variability: an analysis of annual and longer-period signals. Deep Sea Res. I 57, 835–846.

Mooers, C.N.K., 1975. Several effects of a baroclinic current on the cross-stream propagation of inertial-internal waves. Geophys. Fluid Dyn. 6, 245–275.

Mooers, C.N.K., Brooks, D.A., 1977. Fluctuations in the Florida Current, Summer 1970. Deep-Sea Res. 24, 399–425.

Parks, A.B., Shay, L.K., Johns, W.E., Martinez-Pedraja, J., Gurgel, K.-W., 2009. HF radar observations of small-scale surface current variability in the Straits of Florida. J. Geophys. Res. 114, C08002.

Reed, J.K., Messing, C., Walker, B., Brooke, S., Correa, T., Brouwer, M., Udouj, T., 2013. Habitat characterization, distribution, and areal extent of deep-sea coral ecosystem habitat off Florida, southeastern United States. Caribb. J. Sci. 47 (1), 13–30.

Seim, H.E., Winkel, D.P., Gawarkiewicz, G., Gregg, M.C., 1999. A benthic front in the Straits of Florida and its relationship to the structure of the Florida Current. J. Phys. Oceanogr. 29, 3125–3132.

Shay, L.K., Cook, T.M., Haus, B.K., Martinez, J., Peters, H., Van Leer, J., Mariano, A.J., An, P.E., Smith, S., Soloviev, A., Weisberg, R., Luther, M., 2000. VHF Radar detects submesoscale vortex along the Florida Coast. EOS 81, 209–213.

Schott, F., Lee, T.N., Zantopp, R., 1988. Variability of structure and transport of the Florida Current in the period range of days to seasonal. J. Phys. Oceanogr. 18, 1209–1230.

Shearman, R.K., 2005. Observations of near-inertial current variability on the New England shelf. J. Geophys. Res. 110, C02012.

Soloviev, A.V., Luther, M.E., Weisberg, R.H., 2003a. Energetic baroclinic super-tidal oscillations on the shelf off Southeast Florida. Geophys. Res. Lett. 30 (9), 1463.

Soloviev, A.V., Walker, R.J., Weisberg, R.H., Luther, M.E., 2003b. Costal observatory investigates energetic current oscillation on the Southeast Florida shelf. EOS, Transactions 441–450.

Soloviev, A.V., Gilman, M., Young, K., Brusch, S., Lehner, S., 2010. Sonar measurements in ship wakes simultaneous with TerraSAR-X overpasses. Geosci. Remote Sens., IEEE Trans. 48, 841–851.

Stommel, H., 1965. The Gulf Stream—a Physical and Dynamical Description. University of California Press, Berkley, pp. 68 (248 pp).

Wilson, W.D., Johns, W.E., 1997. Velocity structure and transport in the Windward Islands Passages. Deep-Sea Res. 44, 487–520.

Woodson, C.B., 2013. Spatiotemporal variation in cross-shelf exchange across the inner shelf of Monterey Bay, California. J. Phys. Oceanogr. 43, 1648–1665.

Yankovsky, A.E., 2003. The cold water pathway during an upwelling event on the New Jersey shelf. J. Phys. Oceanogr. 33, 1954–1966.

Yankovsky, A.E., Garvine, R.W., 1998. Subinertial dynamics on the inner New Jersey shelf during the upwelling season. J. Phys. Oceanogr. 28, 2444–2458.